HHS Public Access
Author manuscript
Neuroimage. Author manuscript; available in PMC 2017 December 19.

Published in final edited form as:
Neuroimage. 2014 February 01; 86: 221–230. doi:10.1016/j.neuroimage.2013.09.001.

The influence of spatial resolution and smoothing on the detectability of resting-state and task fMRI

Erin K. Molloy[a], **Mary E. Meyerand**[b,c], and **Rasmus M. Birn**[a,c]

[a]Department of Psychiatry, University of Wisconsin Madison, Madison, WI, USA

[b]Department of Biomedical Engineering, University of Wisconsin Madison, Madison, WI, USA

[c]Department of Medical Physics, University of Wisconsin Madison, Madison, WI, USA

Abstract

Functional MRI blood oxygen level-dependent (BOLD) signal changes can be subtle, motivating the use of imaging parameters and processing strategies that maximize the temporal signal-to-noise ratio (tSNR) and thus the detection power of neuronal activity-induced fluctuations. Previous studies have shown that acquiring data at higher spatial resolutions results in greater percent BOLD signal changes, and furthermore that spatially smoothing higher resolution fMRI data improves tSNR beyond that of data originally acquired at a lower resolution. However, higher resolution images come at the cost of increased acquisition time, and the number of image volumes also influences detectability. The goal of our study is to determine how the detection power of neuronally induced BOLD fluctuations acquired at higher spatial resolutions and then spatially smoothed compares to data acquired at the lower resolutions with the same imaging duration. The number of time points acquired during a given amount of imaging time is a practical consideration given the limited ability of certain populations to lie still in the MRI scanner. We compare acquisitions at three different in-plane spatial resolutions (3.50×3.50 mm^2, 2.33×2.33 mm^2, 1.75×1.75 mm^2) in terms of their tSNR, contrast-to-noise ratio, and the power to detect both task-related activation and resting-state functional connectivity. The impact of SENSE acceleration, which speeds up acquisition time increasing the number of images collected, is also evaluated. Our results show that after spatially smoothing the data to the same intrinsic resolution, lower resolution acquisitions have a slightly higher detection power of task-activation in some, but not all, brain areas. There were no significant differences in functional connectivity as a function of resolution after smoothing. Similarly, the reduced tSNR of fMRI data acquired with a SENSE factor of 2 is offset by the greater number of images acquired, resulting in few significant differences in detection power of either functional activation or connectivity after spatial smoothing.

Keywords

functional MRI; resolution; spatial smoothing; SENSE; detection power; functional connectivity

Correspondence to: Rasmus M. Birn, Department of Psychiatry, University of Wisconsin Madison, Madison, WI, 53719, Phone: 608-265-5609, rbirn@wisc.edu.

Introduction

One of the central challenges in functional Magnetic Resonance Imaging (fMRI) is the detection of subtle fluctuations in neuronal activity-induced blood oxygen level-dependent (BOLD) signal in the presence of various sources of noise. This challenge has led to an ongoing effort to increase the spatial and temporal signal-to-noise ratios (SNR) by modifying both acquisition parameters and processing strategies. The spatial SNR reflects the mean signal intensity divided by its variation over space, while the temporal SNR reflects the mean signal intensity divided by its variation over time. Improvements in temporal SNR are limited by physiological noise. Unlike system or thermal noise, variance from cardiac and respiratory pulsations increases with signal strength causing gains in temporal SNR to plateau (Kruger and Glover, 2001).

Acquiring images at higher resolutions lowers the physiological-to-thermal noise ratio and decreases partial volume averaging with non-active tissues. This enables a higher percent signal change or greater contrast-to-noise ratio (CNR) and increases the probability of detecting true positive activation (Bodurka et al., 2007; Hyde et al., 2001; Geissler et al., 2005; Weibull et al., 2008; Newton et al., 2012). Furthermore, Triantafyllou and colleagues have shown that spatially smoothing images from higher resolution acquisitions results in greater temporal SNR than that of images directly acquired at lower resolutions (Triantafyllou et al., 2006). Similarly, the application of a low-pass spatial filter improves the significance of BOLD activation in simulated data suggesting that in many cases physiological noise has a higher spatial frequency content (i.e., is less spatially correlated) than neuronal activity-induced BOLD fluctuations (Lowe and Sorenson, 1997).

These findings suggest that fMRI data should be acquired at higher resolutions in order to improve the detection of subtle BOLD signal changes. However, it has also been demonstrated that the detection of the BOLD response depends strongly on the number of acquired images (Murphy et al., 2007). Lower resolution images can be acquired more quickly allowing more volumes to be collected during the same amount of imaging time. Prior studies investigating the effect of spatial smoothing in fMRI compare different spatial resolutions acquired at the same TR and hence with the same number of volumes, and thus the relative benefit of reducing uncorrelated noise by spatially smoothing higher resolution images versus acquiring more images at lower resolutions remains unexplored. In addition, SENSE acceleration can be utilized to increase the rate of image acquisition but with a loss in temporal SNR (Pruessmann et al., 1999; de Zwart et al., 2002). Finally, these imaging parameters effects on temporal SNR and CNR can be difficult to extend to resting-state functional connectivity, where resting-state fluctuations in brain activity contribute to the variance in the fMRI signal over time and are generally included as part of the “noise” in such calculations.

Because of the multiple complex factors that affect detection power, we perform an empirical study of resolutions that are common in many of our past and current fMRI studies (e.g., 3.50 × 3.50 mm in plane) as well as higher resolution acquisitions that are being considered (e.g., 2.33 × 2.33 mm^2 and 1.75 × 1.75 mm^2), all with and without a SENSE acceleration factor of 2. These resolutions are acquired at their minimum TR for a constant amount of imaging time and are evaluated based on temporal SNR, CNR, and detectability of both task-activation and resting-state functional connectivity. This study is additionally motivated by the increasing popularity of adding quick resting-state scans to existing protocols where resolving extremely fine structures is not always the primary concern, and where spatial smoothing of several millimeters is a common preprocessing step.

Methods

Data Acquisition

Data was collected from eight healthy subjects on a 3.0 T MRI scanner with an 8-channel receive-only RF head coil array (Discovery MR750, General Electric Medical Systems, Milwaukee, WI, USA). Informed consent was obtained from all participants in accordance with a Wisconsin Institutional Review Board (IRB) approved protocol.

Structural images with 1 mm isotropic voxels were acquired axially with an MPRAGE sequence (TE = 3.18 ms, TI = 450 ms, TR = 8.13 ms, flip angle = 12 degrees). For each of the 6 sets of imaging parameters (Table 1), BOLD EPI time series were collected in the sagittal plane (TE = 25 ms, flip angle = 60 degrees, field of view (FOV) = 224 × 224 mm^2, slice thickness = 3.5 mm, number of slices = 40 slices). For each resolution, the minimum TR (rounded to the nearest 50 ms) was chosen to allow the maximum number of volumes to be acquired during a constant amount of scanning time. Phantom experiments were conducted to confirm that spatial and temporal SNR were similar across the planes of acquisition for fMRI volumes acquired with a SENSE acceleration factor of 2. Specifically, spatial SNR was 139 ± 8, 137 ± 8, and 138 ± 7 while temporal SNR was 141 ± 22, 147 ± 22, and 140 ± 21 for the phantom images collected at a resolution of 1.75 × 1.75 mm^2 in the axial, coronal, and sagittal planes, respectively.

Subjects were asked to remain “clear, calm, and awake” as they rested with their eyes closed during the collection of 5-minute fMRI time-courses. In addition, 3-minute fMRI time-courses were collected, during which subjects performed a combined motor and language-processing task. Subjects viewed alternating 20-second intervals of either a fixation cross or a series of words and non-words presented every 2 seconds. Visual information was displayed using fiber optic display goggles (Avotec, Inc., Stuart, FL, USA). Subjects were instructed to rest when viewing the fixation cross and to tap each finger to thumb while covertly deciding whether the word was a member of the English language when viewing text. Resting-state and task fMRI data was collected for each of the six sets of imaging parameters making for a total of 12 scans per subject. The 5-minute resting-state fMRI data for the 3.50 × 3.50 mm^2 acquisition was aborted early for one subject and thus excluded from all analyses. Resting-state scans were collected prior to the task scans, and the order of acquired nominal resolutions was counterbalanced across subjects.

Data Preprocessing

Images were corrected for slice dependent time shifts and motion using the AFNI software package (Cox, 1996), aligned to a T1-weighted structural scan and transformed into Talairach Atlas space (Talairach and Tournoux, 1988) with a single affine transform (Saad et al., 2009), and resampled to 1.75 × 1.75 × 1.75 mm^3 voxels. Data acquired during the first 8 seconds of each run was removed. Data was spatially smoothed using 2D Gaussian kernels to within 1% of an in-plane (sagittal) FWHM of 5.5 mm. A two-way repeated-measures ANOVA (resolution: 3.50 × 3.50 mm^2, 2.33 × 2.33 mm^2, 1.75 × 1.75 mm^2; SENSE: factor of 1, factor of 2) confirmed there was no significant difference in smoothness with p-values of 0.867 and 0.808, respectively. Prior to spatial smoothing, acquisitions with nominal in-plane resolutions of 3.5 × 3.5 mm^2, 2.33 × 2.33 mm^2, and 1.75 × 1.75 mm^2 had an average estimated in-plane FWHM of 4.6 mm, 2.6 mm, and 2.1 mm, respectively. In-plane smoothness was estimated with AFNI's 3dFWHMx.

Signal-Noise-Ratio

Both spatial and temporal SNR was calculated post preprocessing for each subject's linearly de-trended fMRI time-courses both before and after in-plane spatial smoothing but prior to temporal filtering and nuisance regression. Spatial SNR was computed as the ratio of mean fMRI signal over time to the standard deviation of the noise computed over a hand-selected ROI outside of the brain. The standard deviation of the noise was corrected by a factor of 1.43 to account for the 8-channel RF head coil and the sum-of-square image reconstruction (Eq. 4 in Gilbert, 2007; Gonzalez-Castillo et al., 2011). Temporal SNR was computed by dividing the mean of the signal over time by its standard deviation over time. Both spatial and temporal SNR was averaged over 1× eroded cerebral spinal fluid (CSF), gray matter (GM), and white matter (WM) masks as defined by an automated segmentation of the T1-weighted structural scan using FSL's FAST routine (Zhang et al., 2001; Smith et al., 2004; Woolrich et al., 2009).

Task-Activation

The block-design task-activation was modeled using a rectangular function convolved with an ideal hemodynamic response function (Cohen et al. 1997). This generated response function along with constant and linear trends were used in voxel-wise ordinary least squares regression (AFNI's 3dDeconvolve) for preprocessed fMRI time series. The Pearson Correlation Coefficient (R) of each voxel in the resulting statistical parametric maps (SPMs) was converted into a Z-score via the Fisher transform, 1/2*ln((1+R)/(1-R))*sqrt(NT-3), where NT is the number of volumes in the fMRI time-course. CNR (i.e., signal change divided by standard deviation from sources of no-interest) was calculated voxel-wise for each SPM by dividing the task regression coefficients by the standard deviation of the residual error. In order to compare CNR and BOLD signal detectability across resolutions, significantly activate (Bonferroni-corrected, $p < 0.05$) voxels were selected for each subject within a 10 mm radius of the regions involved in language (Brodmann Area 44 and 45), motor (Brodmann Area 4 and 6), and vision (Brodmann Area 17, 18, 19) as defined by AFNI's Talairach Daemon Atlas. Motor and vision ROIs were comprised of voxels that were significantly active in the SPMs from unsmoothed fMRI time series of all 6 imaging parameter combinations (i.e., *intersection*). As the intersection of active voxels in all 6 of the imaging parameters SPMs was empty in Broca's Area, language ROIs were defined as significantly active voxels in the SPMs of at least one of 6 the imaging parameters' unsmoothed fMRI time series (i.e., *union*). CNR and Z-scores were averaged over the task-selected language, motor, and vision ROIs for each subject (Supplementary Figure 1).

Resting-State Functional Connectivity

Given recent publications recognizing head motion's effect on network connectivity in resting-state fMRI (Power et al. 2012; Satterthwaite et al. 2012; Van Dijk et al. 2012), the head motion at each time point was estimated using the 6 rigid-body motion parameters from AFNI's 3dvolreg. The motion (in mm) between consecutive time point *i* and *j* was calculated as the sqrt($(x_j\text{-}x_i)^2 + (y_j\text{-}y_i)^2 + (z_j\text{-}z_i)^2 + (\alpha_j\text{-}\alpha_i)^2 + (\beta_j\text{-}\beta_i)^2 + (\gamma_j\text{-}\gamma_i)^2$), where one degree of rotation at the center of the head is approximately 1 mm of movement at the surface of the head (Kennedy et al., 2008; Jones et al., 2010; Meier et al., 2012; Patriat et al., 2013). Time points with movement from the previous time point greater than or equal to 0.25 mm were censored during resting-state functional connectivity analyses (Power et al. 2012). The 2.33 × 2.33 mm^2 with SENSE factor of 2 and the 1.75 × 1.75 mm^2 acquisitions from one subject were excluded from the analysis due to excessive head motion (greater than 20% of volumes censored).

Functional connectivity was computed using a seed region-based approach (Biswal et al., 1995). Resting-state fMRI time series were temporally filtered (band-pass: 0.01 Hz < f < 0.1 Hz). Seed regions in the left and right motor cortex were defined from each subject's task-selected motor ROI (Task-Activation). Temporally filtered EPI voxel time series were averaged over the task-selected left motor ROI and regressed against all other voxels in the brain (AFNI's 3dDeconvolve) simultaneously with constant and linear trends as well as time series of no-interest (i.e., nuisance regressors - spurious fluctuations unlikely to be of neuronal origin). Specifically, the 12 nuisance regressors included the six rigid-body motion parameters as well as the mean signals and their first derivatives (computed by backward differences) from eroded CSF and 2× eroded WM masks (Jo et al., 2010). The Pearson Correlation Coefficient (R) of each voxel in the resulting SPMs was transformed to a more normal distribution using the Fisher Z transform (Task-Activation) and averaged over the task-selected right motor ROI to gain a measure of within motor network connectivity. This process was repeated to determine connectivity between the task-selected left and right vision ROIs. To examine the specificity of functionally connected regions, Z-scores in SPMs from seeding the task-selected left motor ROI were also averaged over the task-selected vision ROI (Van Dijk et al., 2010). This was used to determine whether a given resolution had greater correlations specifically between regions in known functional networks as oppose to greater correlations globally (i.e., greater correlations also between regions in different functional networks).

Spherical seeds (radius = 4 mm) defined in the left motor cortex (−36, −22, 54), right motor cortex (36, −22, 54), left visual cortex (−30, −85, 4), right visual cortex (30, −85, 4), posterior cingulate (0, −50, 26), and medial prefrontal cortex (0, 50, −8) were used for additional functional connectivity analyses (VanDijk et al., 2010). In order to mimic more conventional resting-state processing, nuisance regression was performed to both smoothed and unsmoothed functional MRI data prior to temporal filtering (bandpass: 0.01 Hz < f < 0.1 Hz) and spatial smoothing with a 3-dimensional Gaussian kernel (FWHM = 6 mm). Finally, left motor to right motor functional connectivity was computed via averaging the post Gaussian smoothed fMRI data within the spherical left motor ROI and regressing the resulting time-course against all other voxels in the brain (AFNI's 3dDeconvolve). The resulting Pearson Correlation Coefficient of each voxel in the resulting SPMs was converted into a Z-score, and the Z-scores were averaged over the spherical right motor ROI. This process was repeated for left to right visual cortex connectivity as well as posterior cingulate (PC) to medial prefrontal cortex (mPFC) connectivity.

Differences as a function of resolution and SENSE acceleration

Spatial SNR values are reported for CSF, GM, and WM for each of the nominal resolutions. Repeated measures ANOVAs (resolution: 3.50×3.50 mm^2, 2.33×2.33 mm^2, 1.75×1.75 mm^2) were used to determine the effect of resolution on spatial SNR. Two-way repeated-measures ANOVAs (resolution: 3.50×3.50 mm^2, 2.33×2.33 mm^2, 1.75×1.75 mm^2; SENSE: factor of 1, factor of 2) were used to determine the effects of resolution and SENSE acceleration on task (Table 1) and resting-state (Table 2) fMRI data both with and without smoothing. P-values less than 0.05 are considered significant.

Results

Unsmoothed task fMRI data

Spatial SNR in the CSF, GM, and WM is respectively 333 ± 64, 292 ± 53, and 267 ± 47 for the 3.50×3.50 mm^2 acquisition, 224 ± 36, 193 ± 26, and 170 ± 26 for the 2.33×2.33 mm^2 acquisition, and 150 ± 24, 127 ± 17, and 111 ± 17 and for the 1.75×1.75 mm^2 acquisition. As expected, spatial SNR in CSF, GM, and WM is significantly increased with decreasing resolutions ($p < 0.03$). Similarly, temporal SNR in CSF, GM, and WM is significantly greater for *lower* resolutions as well as for acquisitions without SENSE acceleration factor of 2 (Figure 1A). The CNR in the task-selected motor ROI is significantly greater for lower resolutions as well as for acquisitions without SENSE acceleration factor of 2 (Figure 1C). Although no significant differences from resolution or SENSE were found for *CNR* within the language or vision ROIs, the *detectability of task-activation* (mean Z-score) is significantly greater for lower resolutions in language, motor, and vision ROIs (Figure 1E, Figure 2, Supplementary Figure 2). The addition of a SENSE factor of 2 did not significantly affect the detectability of task-activation.

Smoothed task fMRI data

Spatial SNR in the smoothed CSF, GM, and WM is respectively 395 ± 88, 348 ± 76, and 321 ± 68 for the 3.50×3.50 mm^2 acquisition, 494 ± 112, 431 ± 91, and 392 ± 86 for the 2.33×2.33 mm^2 acquisition, and 390 ± 74, 334 ± 55, and 303 ± 56 and for the 1.75×1.75 mm^2 acquisition. Differences in spatial SNR in CSF, GM, and WM from resolution are not significant with p-values of 0.052, 0.071, and 0.051, respectively. Temporal SNR in GM and WM is significantly greater in *higher* resolutions as well as for acquisitions without SENSE acceleration factor of 2 (Figure 1B). There are no significant differences in CNR due to resolution or SENSE except for the CNR within the task-selected motor ROI, which is significantly greater for acquisitions without SENSE acceleration factor of 2 (Figure 1D). Lower resolution acquisitions have significantly greater detectability of task-activation in only the task-selected motor and vision ROIs (Figure 1F). Detectability of task activation is significantly higher for a SENSE factor of 1 compared to 2 only within the task-selected motor ROI (Table 2).

Unsmoothed resting-state fMRI data

Spatial SNR in the CSF, GM, and WM is respectively 319 ± 41, 279 ± 27, and 254 ± 25 for the 3.50 × 3.50 mm^2 acquisition, 231 ± 31, 199 ± 21, and 173 ± 21 for the 2.33 × 2.33 mm^2 acquisition, and 141 ± 15, 120 ± 10, and 104 ± 11 and for the 1.75 × 1.75 mm^2 acquisition. Again as expected, spatial SNR in CSF, GM, and WM is significantly different across resolutions ($p < 3E\text{-}04$). Similarly, lower resolution acquisitions as well as acquisitions without SENSE acceleration factor of 2 have greater temporal SNR in GM, CSF, and WM (Figure 3A). Motor and vision functional connectivity between task-selected ROIs is significantly greater for lower resolutions; however, there are no significant differences in between network (task-selected left motor to vision) connectivity (Figure 3C, Figure 4, Supplementary Figure 3).

There were no significant differences in the detectability of functional connectivity computed with task-selected ROIs for a SENSE acceleration factor of 2 compared to 1. Functional connectivity between the PC and mPFC (Figure 5, Supplementary Figure 4) is significantly higher for lower resolutions as well as for acquisitions with SENSE acceleration factor of 2, whereas functional connectivity between the spherical vision ROIs was only significantly greater for lower resolutions. There were no significant differences in motor or vision functional connectivity strength from spherical ROIs due resolution or SENSE (Figure 3E).

Smoothed resting-state fMRI data

Spatial SNR in the CSF, GM, and WM is respectively 373 ± 45, 328 ± 28, and 301 ± 27 for the 3.50 × 3.50 mm^2 acquisition, 530 ± 122, 461 ± 98, and 417 ± 97 for the 2.33 × 2.33 mm^2 acquisition, and 375 ± 65, 323 ± 47, and 291 ± 48 and for the 1.75 × 1.75 mm^2 acquisition. After smoothing, spatial SNR in CSF, GM, and WM does not significantly vary with the resolution of acquisition. Temporal SNR in GM, CSF, and WM is significantly lower for acquisitions with no SENSE acceleration compared to a SENSE acceleration factor of 2 (Figure 3B). There are no significant differences in functional connectivity between any task-selected ROIs due to resolution or SENSE post-smoothing (Figure 3D). The same was true of functional connectivity between spherical ROIs, except that PC to mPFC connectivity was greater for acquisitions with SENSE acceleration factor of 2 (Figure 3F). This could be due to the lower distortion in the prefrontal region for acquisitions with SENSE acceleration.

Discussion

Higher resolution acquisitions as well as acquisitions utilizing a SENSE acceleration factor of 2 come with significant losses in temporal SNR, as expected. This loss is recovered by spatial smoothing; however, these relationships in temporal SNR do not directly translate to CNR or the detectability of either task-activation or functional connectivity, particularly when the total imaging duration is held constant and the TR is allowed to vary. Despite the similarity in temporal SNR, lower resolution acquisitions were slightly better at detecting functional task-activation in the motor and visual cortices. Although a SENSE acceleration factor of 2 significantly reduced the temporal SNR even after spatial smoothing, the detectability of functional activation and connectivity was either not significantly different (for motor and visual areas) or showed a slight improvement (e.g., in the connectivity between mPFC and PC). Consequently, the loss of temporal SNR from SENSE acceleration was balanced by an increase in the number of images that can be acquired in a given amount of time. Although it is not the focus of the current study, it should be noted that SENSE acceleration decreases the echo spacing (ESP) and thus the amount of B_0 field distortion. This allows better alignment of images and may improve group analyses, particularly for higher resolution acquisitions and within regions with greater susceptibility to distortion and signal dropout (e.g., mPFC). In addition, magnetic field gradients in the phase-encoding directions can cause the image to be stretched, resulting in some signal reduction. These distortions, and the associated signal losses, are reduced at lower resolutions and for data acquired with SENSE acceleration.

Prior studies comparing the temporal SNR of acquisitions at different resolution both with and without smoothing used a constant TR and/or number of volumes for all resolutions. In our study, the TR is allowed to vary across different across resolutions. This allows for a greater number of volumes to be acquired at lower resolutions, improving detectability of activation, but also leads to differences in the MRI signal due to the T1 relaxation. The lower resolution acquisitions have a shorter TR and therefore a shorter time for T1 recovery than if they were acquired at the same TR as the higher resolution acquisitions. This shorter TR results in a reduction in signal for the lower resolution acquisitions, biasing the detection of activation and connectivity in favor of higher resolution acquisitions. Similarly, shorter TRs can lead to greater physiological noise, e.g. from greater in-flow effects. However, even with these biases towards higher resolutions, we do not see a significant increase in detection power for higher resolution acquisitions.

The contribution of physiological noise also depends on the flip angle. In the current study, the flip angle was held constant. An interesting question is whether similar finding would be obtained at a different flip angle, or when the flip angle is varied across TRs (e.g. set to the Ernst angle). A recent study by Gonzalez-Castillo shows that the temporal SNR is relatively insensitive to the flip angle across a wide range of flip angles (Gonzalez-Castillo et al., 2011). However, the proportion of physiological noise does vary with the flip angle, with flip angles closer to the Ernst angle having a greater ratio of physiological to thermal noise. A theoretical estimation of the changes in tSNR and detectability by spatial smoothing (see Appendix) suggests that for the sSNR and resolutions tested in our study, the effect of changing the flip angle from 60 degrees to the Ernst angle for each TR would improve the tSNR and detectability, but that the detectability would still be lower for the smoothed higher resolution acquisitions.

A challenge when comparing signal characteristics across different sets of imaging parameters is that the comparisons are necessarily performed between separate runs. Variations in task performance, attention, or subject motion between runs can affect the temporal SNR, CNR, and detection power. While compliance or attention levels during the task were not monitored, the order of acquired parameters were counterbalanced across subjects, and we have no reason to expect that there would be systematic differences in compliance or attention for different imaging parameters.

Recent technological and methodological improvements, such as multiband imaging (Larkman et al., 2001; Feinberg et al., 2010; Moeller et al., 2010; Setsompop et al., 2012), allow image volumes to be acquired much more rapidly. The increased number of images that can be acquired in a fixed amount of time with these sequences will likely greatly improve the detection power of both task activation and functional connectivity. However, even within multiband acquisitions, tradeoffs exist between the improvements afforded by higher spatial resolutions and the greater number of image volumes that can be acquired at lower spatial resolutions.

Conclusion

Consistent with previous studies, spatial smoothing greatly improves the temporal SNR and detection power of neuronal activity-induced BOLD fMRI signal changes, particularly for acquisitions at high spatial resolutions. However, our data shows that after spatially smoothing the data to the same intrinsic smoothness, the detection power of task-related BOLD signal changes is slightly higher for lower resolution acquisitions in some brain areas (e.g., in motor and vision areas), but not significantly different across the various tested resolutions in other areas (e.g. in Broca's area). Furthermore, after spatial smoothing, we found no significant differences in functional connectivity either computed from task-selected ROIs or traditional spherical ROIs as a function of spatial resolution. Consequently, studies may wish to have the flexibility to capitalize on the improved ability to resolve fine spatial structures and increased specificity (Yoo et al. 2004; Soltysik and Hyde 2008) from higher resolution fMRI data. Similarly, the reduced temporal SNR of fMRI data acquired with a SENSE acceleration factor of 2 is offset by the greater number of images collected, resulting in few significant differences in detection power of either functional activation or connectivity after spatial smoothing.

Supplementary Material

Refer to Web version on PubMed Central for supplementary material.

Acknowledgments

We thank Steven R. Kecskemeti and Jerzy Bodurka for helpful discussions. This research was supported by the Health Emotions Research Institute and NIH grant RC1MH090912.

References

Biswal B, Yetkin FZ, Haughton VM, Hyde JS. Functional connectivity in the motor cortex of resting human brain using echo-planar MRI. Magnetic Resonance in Medicine. 1995; 34(4):537–541. [PubMed: 8524021]

Bodurka J, Ye F, Petridou N, Murphy K, Bandettini PA. Mapping the MRI voxel volume in which thermal noise matches physiological noise--implications for fMRI. Neuroimage. 2007; 34(2):542–549. [PubMed: 17101280]

Cohen JD, Perlstein WM, Braver TS, Nystrom LE, Noll DC, Jonides J, Smith EE. Temporal dynamics of brain activation during a working memory task. Nature. 1997; 386(6625):604–608. [PubMed: 9121583]

Cox RW. AFNI: software for analysis and visualization of functional magnetic resonance neuroimages. Computers & Biomedical Research. 1996; 29(3):162–173. [PubMed: 8812068] de Zwart JA, van Gelderen P, Kellman P, Duyn JH. Application of sensitivity-encoded echo-planar imaging for blood oxygen level-dependent functional brain imaging. Magn Reson Med. 2002; 48(6):1011–1020. [PubMed: 12465111]

Edelstein WA, Glover GH, Hardy CJ, Redington RW. The intrinsic signal-to-noise ratio in NMR imaging. Magn Reson Med. 1986; 3(4):604–618. [PubMed: 3747821]

Feinberg D, Moeller S, Smith S, Auerbach E, Ramanna S, Glasser M, Miller K, Ugurbil K, Yacoub E. Multiplexed echo planar imaging for sub-second whole brain FMRI and fast diffusion imaging. PLoS ONE. 2010; 5(12):e15710. [PubMed: 21187930]

Geissler A, Lanzenberger R, Barth M, Tahamtan AR, Milakara D, Gartus A, Beisteiner R. Influence of fMRI smoothing procedures on replicability of fine scale motor localization. Neuroimage. 2005; 24(2):323–331. [PubMed: 15627575]

Gilbert G. Measurement of signal-to-noise ratios in sum-of-squares MR images. J Magn Reson Imaging. 2007; 26(6):1678. author reply 1679. [PubMed: 18059007]

Gonzalez-Castillo J, Roopchansingh V, Bandettini PA, Bodurka J. Physiological noise effects on the flip angle selection in BOLD fMRI. Neuroimage. 2011; 54(4):2764–2778. [PubMed: 21073963]

Hyde JS, Biswal BB, Jesmanowicz A. High-resolution fMRI using multislice partial k-space GR-EPI with cubic voxels. Magn Reson Med. 2001; 46(1):114–125. [PubMed: 11443717]

Jo HJ, Saad ZS, Simmons WK, Milbury LA, Cox RW. Mapping sources of correlation in resting state FMRI, with artifact detection and removal. Neuroimage. 2010; 52(2):571–582. [PubMed: 20420926]

Jones TB, Bandettini PA, Kenworthy L, Case LK, Milleville SC, Martin A, Birn RM. Sources of group differences in functional connectivity: an investigation applied to autism spectrum disorder. Neuroimage. 2010; 49:401–414. [PubMed: 19646533]

Kennedy DP, Courchesne E. The intrinsic functional organization of the brain is altered in autism. Neuroimage. 2008; 39:1877–1885. [PubMed: 18083565]

Kruger G, Glover GH. Physiological noise in oxygenation-sensitive magnetic resonance imaging. Magn Reson Med. 2001; 46(4):631–637. [PubMed: 11590638]

Larkman DJ, Hajnal JV, Herlihy AH, Coutts GA, Young IR, Ehnholm G. Use of multicoil arrays for separation of signal from multiple slices simultaneously excited. J Magn Reson Imaging. 2001; 13(2):313–7. [PubMed: 11169840]

Lowe MJ, Sorenson JA. Spatially filtering functional magnetic resonance imaging data. Magn Reson Med. 1997; 37(5):723–729. [PubMed: 9126946]

Moeller S, Yacoub E, Olman CA, Auerbach E, Strupp J, Harel N, Ugurbil K. Multiband multislice GE-EPI at 7 tesla, with 16-fold acceleration using partial parallel imaging with application to high spatial and temporal whole-brain fMRI. Magn Reson Med. 2010; 63(5):1144–53. [PubMed: 20432285]

Murphy K, Bodurka J, Bandettini PA. How long to scan? The relationship between fMRI temporal signal to noise ratio and necessary scan duration. Neuroimage. 2007; 34(2):565–574. [PubMed: 17126038]

Newton AT, Rogers BP, Gore JC, Morgan VL. Improving measurement of functional connectivity through decreasing partial volume effects at 7 T. Neuroimage. 2012; 59(3):2511–2517. [PubMed: 21925611]

Power JD, Barnes KA, Snyder AZ, Schlaggar BL, Petersen SE. Spurious but systematic correlations in functional connectivity MRI networks arise from subject motion. Neuroimage. 2012; 59(3):2142–2154. [PubMed: 22019881]

Pruessmann KP, Weiger M, Scheidegger MB, Boesiger P. SENSE: sensitivity encoding for fast MRI. Magn Reson Med. 1999; 42(5):952–962. [PubMed: 10542355]

Saad ZS, Glen DR, Chen G, Beauchamp MS, Desai R, Cox RW. A new method for improving functional-to-structural MRI alignment using local Pearson correlation. Neuroimage. 2009; 44(3): 839–848. [PubMed: 18976717]

Satterthwaite TD, Wolf DH, Loughead J, Ruparel K, Elliott MA, Hakonarson H, Gur RC, Gur RE. Impact of in-scanner head motion on multiple measures of functional connectivity: relevance for studies of neurodevelopment in youth. Neuroimage. 2012; 60(1):623–632. [PubMed: 22233733]

Scouten A, Papademetris X, Constable RT. Spatial resolution, signal-to-noise ratio, and smoothing in multi-subject functional MRI studies. Neuroimage. 2006; 30(3):787–793. [PubMed: 16343951]

Setsompop K, Gagoski BA, Polimeni JR, Witzel T, Wedeen VJ, Wald LL. Blipped-controlled aliasing in parallel imaging for simultaneous multislice echo planer imaging with reduced g-factor penalty. Magnetic Resonance in Medicine. 2012; 67(5):1210–1224. [PubMed: 21858868]

Smith SM, Jenkinson M, Woolrich MW, Beckmann CF, Behrens TE, Johansen-Berg H, Bannister PR, De Luca M, Drobnjak I, Flitney DE, Niazy RK, Saunders J, Vickers J, Zhang Y, De Stefano N, Brady JM, Matthews PM. Advances in functional and structural MR image analysis and implementation as FSL. Neuroimage. 2004; 23(1 Suppl):S208–219. [PubMed: 15501092]

Soltysik DA, Hyde JS. High spatial resolution increases the specificity of block-design BOLD fMRI studies of overt vowel production. Neuroimage. 2008; 41(2):389–397. [PubMed: 18387825]

Talairach, J., Tournoux, P. Co-Planar Stereotaxic Atlas of the Human Brain. New York: Thieme Medical Publishers, Inc; 1988.

Triantafyllou C, Hoge RD, Wald LL. Effect of spatial smoothing on physiological noise in high-resolution fMRI. Neuroimage. 2006; 32(2):551–557. [PubMed: 16815038]

Van Dijk KR, Hedden T, Venkataraman A, Evans KC, Lazar SW, Buckner RL. Intrinsic functional connectivity as a tool for human connectomics: theory, properties, and optimization. J Neurophysiol. 2010; 103(1):297–321. [PubMed: 19889849]

Van Dijk KR, Sabuncu MR, Buckner RL. The influence of head motion on intrinsic functional connectivity MRI. Neuroimage. 2012; 59(1):431–438. [PubMed: 21810475]

Weibull A, Gustavsson H, Mattsson S, Svensson J. Investigation of spatial resolution, partial volume effects and smoothing in functional MRI using artificial 3D time series. Neuroimage. 2008; 41(2): 346–353. [PubMed: 18400520]

Woolrich MW, Jbabdi S, Patenaude B, Chappell M, Makni S, Behrens T, Beckmann C, Jenkinson M, Smith SM. Bayesian analysis of neuroimaging data in FSL. Neuroimage. 2009; 45(1 Suppl):S173–186. [PubMed: 19059349]

Yoo SS, Talos IF, Golby AJ, Black PM, Panych LP. Evaluating requirements for spatial resolution of fMRI for neurosurgical planning. Hum Brain Mapp. 2004; 21(1):34–43. [PubMed: 14689508]

Zhang Y, Brady M, Smith S. Segmentation of brain MR images through a hidden Markov random field model and the expectation-maximization algorithm. IEEE Trans Med Imaging. 2001; 20(1):45–57. [PubMed: 11293691]

Bodurka J, Ye F, Petridou N, Murphy K, Bandettini PA. Mapping the MRI voxel volume in which thermal noise matches physiological noise--implications for fMRI. Neuroimage. 2007; 34:542–549. [PubMed: 17101280]

Gonzalez-Castillo J, Roopchansingh V, Bandettini PA, Bodurka J. Physiological noise effects on the flip angle selection in BOLD fMRI. Neuroimage. 2011; 54:2764–2778. [PubMed: 21073963]

Jones TB, Bandettini PA, Kenworthy L, Case LK, Milleville SC, Martin A, Birn RM. Sources of group differences in functional connectivity: an investigation applied to autism spectrum disorder. Neuroimage. 2010; 49:401–414. [PubMed: 19646533]

Kennedy DP, Courchesne E. The intrinsic functional organization of the brain is altered in autism. Neuroimage. 2008; 39:1877–1885. [PubMed: 18083565]

Kruger G, Glover GH. Physiological noise in oxygenation-sensitive magnetic resonance imaging. Magn Reson Med. 2001; 46:631–637. [PubMed: 11590638]

Meier TB, Desphande AS, Vergun S, Nair VA, Song J, Biswal BB, Meyerand ME, Birn RM, Prabhakaran V. Support vector machine classification and characterization of age-related reorganization of functional brain networks. Neuroimage. 2012; 60:601–613. [PubMed: 22227886]

Patriat R, Molloy EK, Meier TB, Kirk GR, Nair VA, Meyerand ME, Prabhakaran V, Birn RM. The effect of resting condition on resting-state fMRI reliability and consistency: A comparison between resting with eyes open, closed, and fixated. Neuroimage. 2013

Triantafyllou C, Hoge RD, Wald LL. Effect of spatial smoothing on physiological noise in high-resolution fMRI. Neuroimage. 2006; 32:551–557. [PubMed: 16815038]

Appendix

A number of previous studies have shown that the temporal signal to noise ratio (tSNR) is limited by the presence of physiological noise, since this noise scales with the signal (Kruger et al., 2001; Triantafyllou et al., 2006; Bodurka et al., 2007; Gonzalez-Castillo et al., 2011). If we define this scaling factor as λ, such that $\sigma_p = \lambda S$, then the tSNR can be written as,

$$tSNR=\frac{SNR}{\sqrt{1+\lambda^2 SNR^2}} \quad [1]$$

Where SNR is the spatial signal to noise ratio.

When the image is spatially smoothed, then in the best case scenario (i.e. if physiological noise is spatially uncorrelated, Eq. 4 from (Triantafyllou et al., 2006)), the tSNR can be expressed as,

$$tSNR_{smooth}=\sqrt{V}\frac{SNR_{high}}{\sqrt{1+\lambda^2 SNR_{high}{}^2}} \quad [2]$$

Where V is the amount of smoothing, and SNR_{high} is the SNR of the higher resolution image, prior to smoothing. A primary question of interest is how this smoothed tSNR compares to the tSNR of data acquired at a lower resolution. Since SNR_{low} = V SNR_{high} (Eq. 4, (Bodurka et al., 2007)), Equation 2 becomes,

$$tSNR_{smooth}=\frac{SNR_{low}}{\sqrt{V+\frac{\lambda^2}{V} SNR_{low}{}^2}} \quad [3]$$

For comparison, the tSNR of the low resolution image is,

$$tSNR_{low}=\frac{SNR_{low}}{\sqrt{1+\lambda^2 SNR_{low}{}^2}} \quad [4]$$

Note that in the absence of physiological noise, λ=0, and the tSNR for smoothed higher resolution data is reduced by a factor sqrt(V) compared to acquiring the data at higher resolutions.

$$tSNR_{smooth,nophysio}=\frac{SNR_{low}}{\sqrt{V}} \quad [5]$$

Note also that smoothing reduces the contribution of physiological noise. In regimes where physiological noise dominates, this can lead to an increase in tSNR. The detection power, of course, depends not only on the temporal SNR, but also on the number of acquired data points. Therefore, the detection power, D, can be written as:

$$D_{smooth}=\frac{k}{\sqrt{TR}}\frac{SNR_{low}}{\sqrt{V+\frac{\lambda^2}{V}SNR_{low}{}^2}} \quad [6]$$

Where k is a proportionality constant. If the data were acquired as quickly as possible (i.e. with the minimum TE and TR), then TR would be proportional to V, and equation 6 becomes,

$$D_{smooth}=\frac{k_2 SNR_{low}}{\sqrt{V^2+\lambda^2 SNR_{low}{}^2}} \quad [7]$$

Where k_2 is a proportionality constant. Note that in this case, the detection power of smoothed higher resolution data is always lower than the detection power of data acquired at the lower resolution, regardless of the amount of smoothing, SNR, or λ. However, a relatively long echo time (~30ms at 3T) is usually desired in fMRI, limiting the reduction in TR at lower resolutions.

When the influence of flip angle, TR, and T1 are included, equation 3 becomes (Gonzalez-Castillo et al., 2011),

$$tSNR_{smooth}=\frac{SNR_{low}F(\theta,TR,T1)}{\sqrt{V+\frac{\lambda^2}{V}SNR_{low}{}^2F(\theta,TR,T1)^2}} \quad [8]$$

where

$$F(\theta,TR,T1)=\frac{\left(1-e^{-TR/T1}\right)\sin(\theta)}{1-e^{-TR/T1}\cos(\theta)} \quad [9]$$

Similarly, the detection power, D, can be written as:

$$D_{smooth}=\frac{k}{\sqrt{TR}}\frac{SNR_{low}F(\theta_{high},TR_{high},T1)}{\sqrt{V+\frac{\lambda^2}{V}SNR_{low}{}^2F(\theta_{high},TR_{high},T1)^2}} \quad [10]$$

$$D_{low}=\frac{k}{\sqrt{TR}}\frac{SNR_{low}F(\theta_{low},TR_{low},T1)}{\sqrt{1+\lambda^2SNR_{low}{}^2F(\theta_{low},TR_{low},T1)^2}} \quad [11]$$

For SNR=279, λ=0.0075, T1=1340ms, a flip angle of 60 degrees, and the TRs used in the current study, the tSNR for a spatially smoothed 128×128 acquisition will actually be quite similar to the tSNR for the lower resolution 64×64 acquisition, consistent with our observations for the resting-state data. However, according to equations 10 and 11, the detectability for the smoothed higher resolution acquisition is 28% lower than the detectability of the unsmoothed lower resolution acquisition. Setting the flip angle to the Ernst angle for each TR (instead of keeping it fixed at 60 degrees) would, according to equation 8, improve the tSNR of the higher resolution acquisition by 10%, but the detectability of the higher resolution acquisition would only improve by 5% and thus still be 23% lower than the detectability of the lower resolution acquisition.

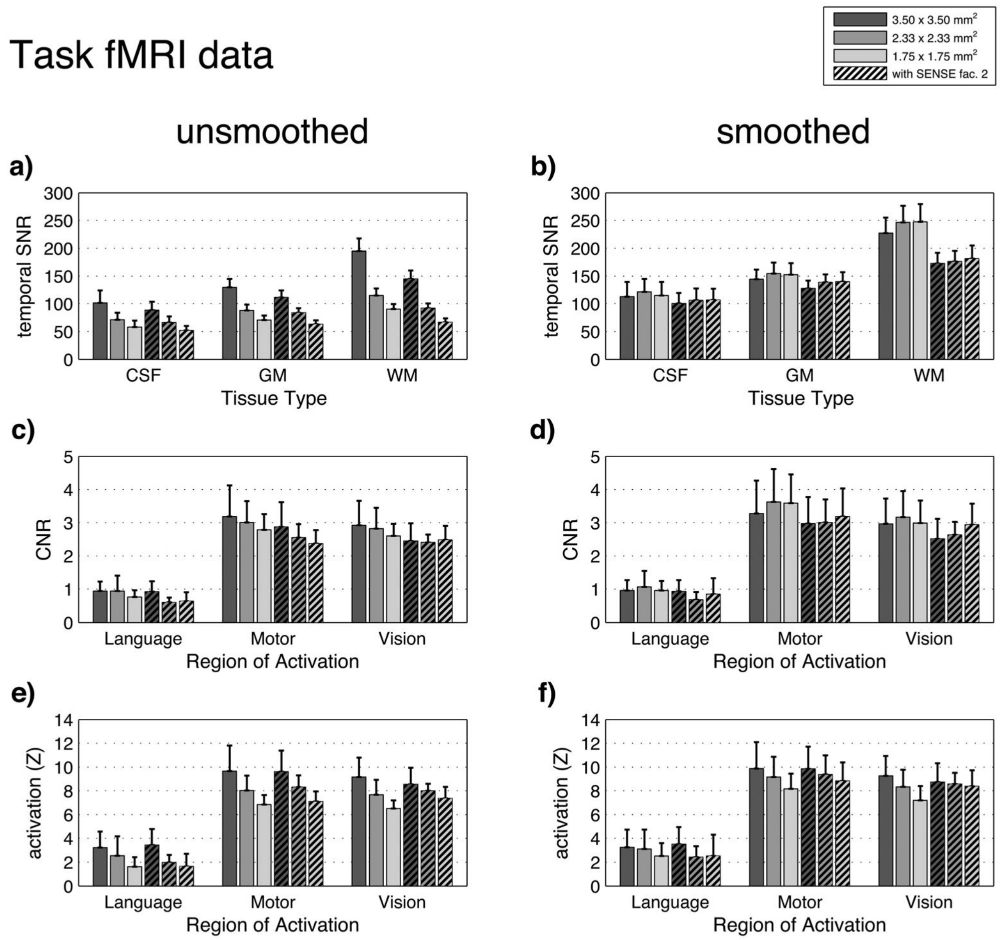

Figure 1.

Temporal SNR, CNR, and task-activation (mean Z-Score) are shown for unsmoothed and smoothed task fMRI data on the right and left, respectively. Temporal SNR (A and B) is shown for cerebral spinal fluid (CSF), grey matter (GM), and white matter (WM) masks. CNR (C and D) and task-activation (E and F) is shown for ROIs selected from task-activation in the language, motor, and vision-processing regions as described in Methods, Task-Activation. Bar graphs are data are averaged across 8 subjects. Error bars indicate the standard deviation across subjects. Imaging parameters with a SENSE acceleration factor of 2 are depicted with stripes.

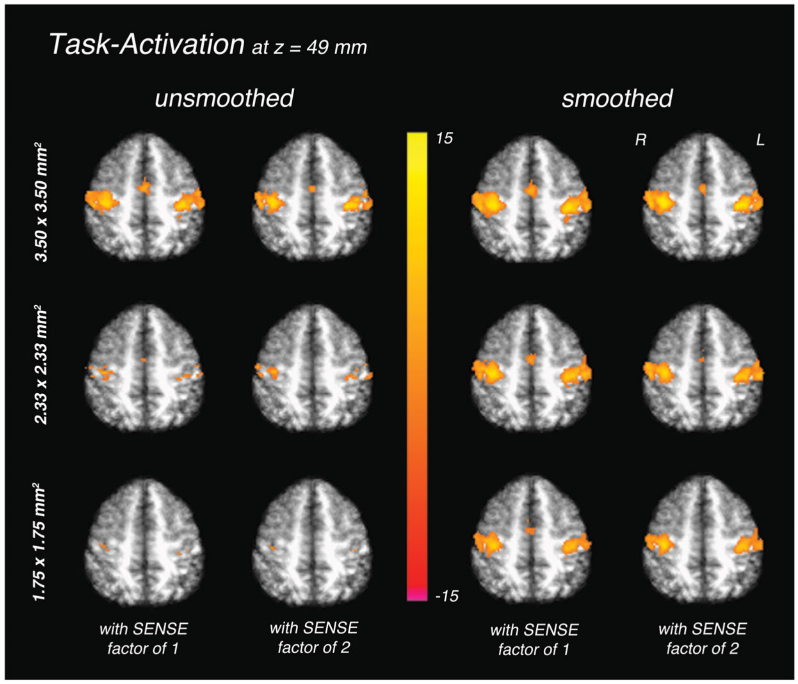

Figure 2.

For each of the six imaging parameters, task-activation is depicted averaged across all eight subjects. Group maps from unsmoothed and smoothed task fMRI data are on the left and right, respectively, and shown at Talairach coordinate z = 49 mm (RAI) for Z-scores greater than 4.

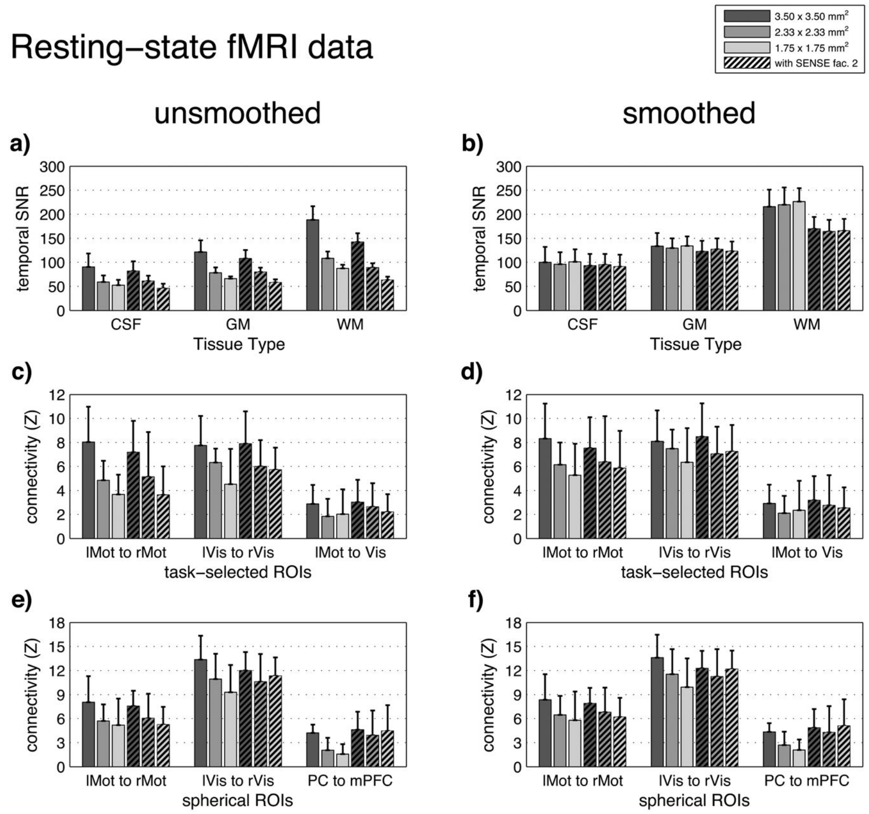

Figure 3.

Temporal SNR, CNR, and task-activation (mean Z-Score) are shown for unsmoothed and smoothed resting-state fMRI data on the right and left, respectively. Temporal SNR (A and B) is shown for cerebral spinal fluid (CSF), grey matter (GM), and white matter (WM) masks. Resting-state functional connectivity (mean Z-score) is shown for both task-selected and spherical ROIs, as described in Methods, Functional Connectivity. Bar graphs are data are averaged across 8 subjects. Error bars indicate the standard deviation across subjects. Imaging parameters with a SENSE acceleration factor of 2 are depicted with stripes.

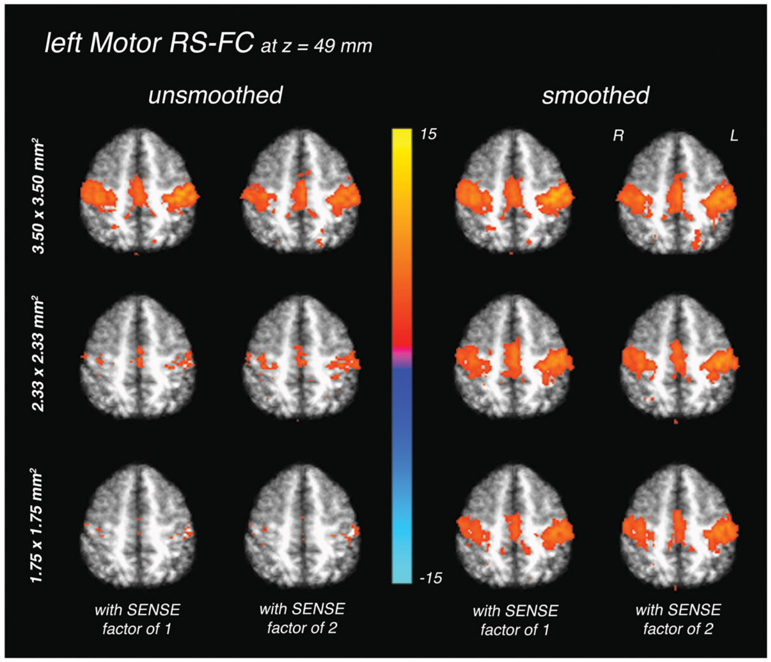

Figure 4.

For each of the six imaging parameters, task-selected left Motor ROI resting-state functional connectivity (RS-FC) is depicted averaged across all eight subjects (excluding the scan aborted early or corrupted by motion; see Methods). Group maps from unsmoothed and smoothed task fMRI data are on the left and right, respectively, and shown at Talairach coordinate z = 49 mm (RAI) for Z-scores greater than 3.

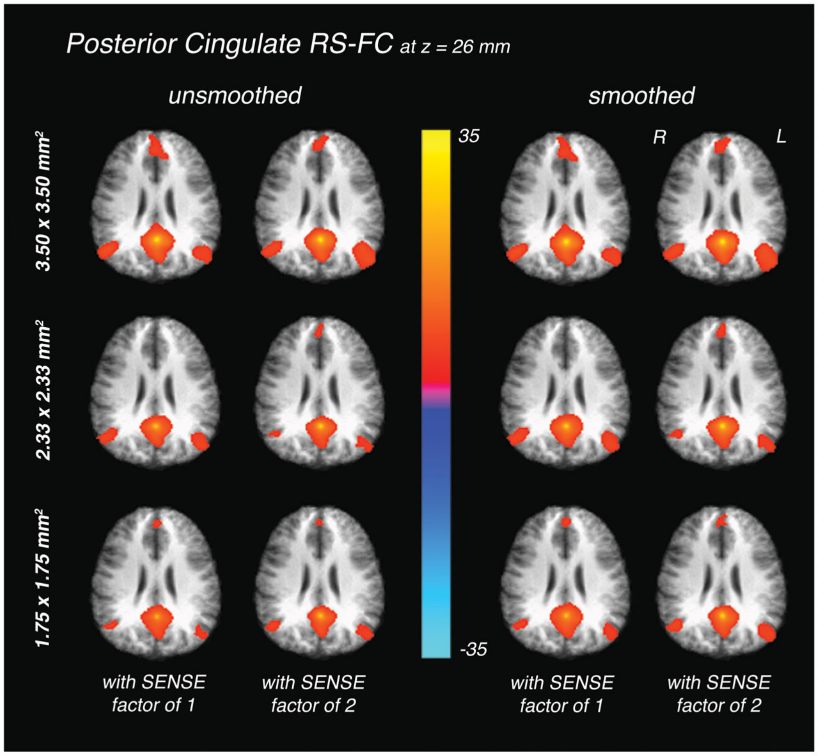

Figure 5.

For each of the six imaging parameters, posterior cingulate (PC) resting-state functional connectivity (RS-FC) is depicted averaged across all eight subjects (excluding the scan aborted early or corrupted by motion; see Methods). Group maps from unsmoothed and smoothed task fMRI data are on the left and right, respectively, and shown at Talairach coordinate z = 26 mm (RAI) for Z-scores greater than 5.

Table 1

Acquisition parameters for both 3-minute task and 5-minute resting-state fMRI time-courses. The minimum repetition time (TR) rounded to the nearest 50 ms was used for each nominal resolution. A sensitivity encoding (SENSE) acceleration factor of one is equivalent to imaging without SENSE. ESP is the echo spacing, and NT is the number of time points or volumes.

Resolution (mm^2)	Matrix	SENSE factor	ESP (ms)	TR (ms)	NT (3 min)	NT (5 min)
3.5 × 3.5	64 × 64	1	0.468	2250	80	134
3.5 × 3.5	64 × 64	2	0.236	2000	90	150
2.33 × 2.33	96 × 96	1	0.616	3000	60	100
2.33 × 2.33	96 × 96	2	0.310	2250	80	134
1.75 × 1.75	128 × 128	1	0.740	3750	48	80
1.75 × 1.75	128 × 128	2	0.372	2750	66	110

Author Manuscript
Author Manuscript
Author Manuscript

Table 2

P-values from two-way repeated measures ANOVAs on the number of resolution (categories: 3.50 × 3.50 mm^2, 2.33 × 2.33 mm^2, 1.75 × 1.75 mm^2) and SENSE acceleration (categories: factor of 1, factor of 2) for both unsmoothed and smoothed functional MRI data from a 3-minute combined language and motor task. Asterisks indicate significance ($p < 0.05$).

Task fMRI data	unsmoothed			smoothed		
	resolution	**SENSE**	**interaction**	**resolution**	**SENSE**	**interaction**
temporal Signal-to-Noise Ratio						
CSF (1× eroded)	1.01E-08*	1.00E-03*	2.01E-02*	0.106	5.83E-04*	9.79E-02
GM (1× eroded)	1.06E-10*	4.65E-04*	2.87E-04*	3.04E-02*	2.15E-04*	0.591
WM (1× eroded)	7.15E-13*	4.69E-07*	1.35E-06*	3.49E-02*	9.11E-08*	1.64E-02*
Contrast-to-Noise Ratio						
language	0.252	0.101	0.229	0.899	0.181	0.241
motor	1.30E-02*	4.33E-03*	0.702	8.98E-02	1.98E-03*	0.381
vision	0.608	0.106	0.365	0.345	0.138	0.348
Task Activation (mean Z-score)						
language	3.31E-02*	0.700	0.468	0.400	0.703	0.457
motor	4.74E-06*	0.399	0.633	7.10E-04*	4.69E-02*	0.374
vision	3.40E-02*	0.633	8.55E-02*	1.19E-02*	0.473	0.108

Table 3

P-values from two-way repeated measures ANOVAs on the number of resolution (categories: 3.50×3.50 mm^2, 2.33×2.33 mm^2, 1.75×1.75 mm^2) and SENSE acceleration (categories: factor of 1, factor of 2) for both unsmoothed and smoothed functional MRI data from 5-minutes resting-state. Asterisks indicate significance ($p < 0.05$).

Resting-state fMRI data	**unsmoothed**			**smoothed**		
	resolution	**SENSE**	**interaction**	**resolution**	**SENSE**	**interaction**
temporal Signal-to-Noise Ratio						
CSF (1× eroded)	1.05E-07*	1.90E-02*	0.305	0.511	1.35E-02*	0.868
GM (1× eroded)	6.75E-09*	1.46E-02*	0.368	0.922	0.240E-02*	0.963
WM (1× eroded)	1.32E-12*	1.54E-06*	1.13E-02	0.853	3.06E-08*	0.279
Task-selected ROIs:						
Functional Connectivity (mean Z-score)						
left motor to right motor	4.42E-03*	0.779	0.943	0.173	0.983	0.993
left vision to right vision	2.14E-02*	0.414	0.348	0.220	0.365	0.488
left motor to right & left vision	0.233	0.595	0.926	0.422	0.685	0.835
Spherical ROIs:						
Functional Connectivity (mean Z-score)						
left motor to right motor	9.55E-02	0.881	0.842	0.285	0.974	0.942
left vision to right vision	3.93E-02*	0.823	0.150	0.127	0.941	0.128
PC to mPFC	3.34E-02*	1.47E-02*	0.115	0.134	1.59E-02*	0.129